Grasping-Force-Based Passive Safety Method for a Vascular Interventional Surgery Robot System

Yonggan Yan, *Graduate Student Member, IEEE*, Shuxiang Guo, *Fellow, IEEE*, Zhijun Lin, *Graduate Student Member, IEEE*, Chuqiao Lyu, *Graduate Student Member, IEEE*, Duohao Zhao, *Graduate Student Member, IEEE*, Pengfei Yang, Yongwei Zhang, Yongxin Zhang, and Jianmin Liu

***Abstract*— Robot-assisted vascular interventional surgery (VIS) changes the surgeons' original operation, which affects their judgment and surgical safety. Therefore, the reliable safety method for robot-assisted surgery is practically valuable. However, the existing active safety methods have two challenges: the difficulty in setting inserting force thresholds suitable for the current vascular environment and the response delay caused by program processing. This article improved a series elastic actuator (SEA)-based guidewire manipulator with an adjustable grasping force function. A multifunctional finger pulp was designed to measure the guidewire inserting force and perceive the manipulating state between fingers simultaneously. Then, an orthogonal force coupling model based on the mechanical–molecular friction theory was established to demonstrate the friction mechanism of cylindrical surgical instruments grasped by elastic grasping surfaces. Based on the model, a passive safety method was proposed to adjust the grasping force autonomously, which can satisfy the inserting force requirements of the phase delivery task and control the safety threshold suitable for the current environment. The evaluation experimental results demonstrated that the designed robot system could manipulate the guidewire accurately. Then the friction experiments verified the designed orthogonal force coupling model. Finally, the in vitro experiments were performed to demonstrate that the designed passive safety method can automatically adjust the grasping force based on the inserting states of the guidewire, reduce the contact force with the vessels, and ensure surgical safety in real-time.**

***Index Terms*— Passive safety, PG2, robot-assisted surgery, safety method, vascular interventional surgery (VIS) robot.**

Manuscript received 9 May 2023; revised 27 July 2023; accepted 11 August 2023. Date of publication 28 August 2023; date of current version 14 September 2023. This work was supported in part by the National High-Tech Research and Development Program (863 Program) of China under Grant 2015AA043202. The Associate Editor coordinating the review process was Dr. Gabriele Patrizi. *(Corresponding author: Shuxiang Guo.)*

Yonggan Yan, Zhijun Lin, Chuqiao Lyu, and Duohao Zhao are with the School of Life Science, Beijing Institute of Technology, Beijing 100081, China.

Shuxiang Guo is with the School of Life Science and the Key Laboratory of Convergence Medical Engineering System and Healthcare Technology, Ministry of Industry and Information Technology, Beijing Institute of Technology, Beijing 100081, China, and also with the Department of Electronic and Electrical Engineering, Southern University of Science and Technology, Shenzhen, Guangdong 518055, China (e-mail: guoshuxiang@bit.edu.cn).

Pengfei Yang, Yongwei Zhang, Yongxin Zhang, and Jianmin Liu are with the Neurovascular Center, Changhai Hospital, Naval Medical University, Shanghai 200433, China.

Digital Object Identifier 10.1109/TIM.2023.3309365

I. Introduction

CARDIOVASCULAR and cerebrovascular diseases have become the first killer affecting human health besides infectious diseases [1], [2]. Vascular interventional surgery (VIS) has become the main treatment because of its small trauma and quick recovery [3], [4]. However, surgeons need to bear X-ray radiation during the operation, which greatly affects their health [5]. The leader–follower robot-assisted surgery solves this problem. Surgeons can remotely control the follower robot to perform surgery outside the operating room to avoid radiation damage [6], [7], [8]. In traditional surgery, to ensure surgical safety, surgeons need to perceive the delivery state of the guidewire in real-time for decision-making and operation. Therefore, many studies focus on establishing more realistic force feedback on the leader side so surgeons can accurately perceive the operation state remotely [4], [8], [9], [10], [11]. However, the operating handles of the leader side are often different from the real surgical devices. It is difficult for surgeons to accurately and timely judge the operation state based on the obtained incomplete information. Then it results in limited improvement in the safety of remote surgery. The follower side of the VIS robot can accurately collect guidewire information in real-time, including image, operating position, force data, and so on [12], [13], [14]. Therefore, the safety methods based on the above information have become one of the important research directions to ensure surgical safety, and substantial achievements have been witnessed [10], [15], [16], [17], [18], [19], [20], [21]. Yan et al. [15] proposed a multi-states' prediction model based on the guidewire inserting force and position data. Based on the model, the human–machine trust was evaluated to adjust the leader–follower mapping ratio online, thereby improving surgical safety and efficiency. Bao et al. [17] first proposed a multilevel operation strategy and designed the corresponding level safety interventions to reduce blood vessel danger. Shi et al. [18] proposed a haptic catheter operating system with operational force amplification. To detect the surgical risk, they proposed a proximal-force-based collision detection algorithm using the z-scores statistical method. Jin et al. [10], [19] designed a miniature force sensor placed at the tip of the catheter to directly measure the contact force between the catheter and the vessel wall. They proposed an active suppression method for surgical risk behavior to improve surgical safety. It has

the potential to predict surgical risk and plan insertion path based on surgical instrument images. Lyu et al. [20] built a GCCM-net model to identify collision between the guidewire tip and the vascular wall and designed a force feedback method based on the deformation features of the guidewire. Zhu et al. [21] proposed a multistage framework for guidewire tip tracking. Furthermore, a guidewire tip fold-back bending detection method and a bending energy calculation method were designed for operation safety. However, to the best of the author's knowledge, almost all the existing safety methods for the robot-assisted surgery are active safety methods. Based on the collected images, force, and position data, they can judge the inserting states of surgical instruments relying on the processing of the logical CPU. Then the robot system carries out the designed interventions to reduce surgical danger. On one hand, active safety methods will inevitably cause trigger delays due to factors such as leader–follower communication, sensors' communication, motors' drive, and model calculations, resulting in untimely safety interventions. On the other hand, the existing active safety methods are difficult to apply to the unstructured, complex vascular environment, and the key parameters need to be set experimentally or empirically [17]. Therefore, the versatility is limited.

During the insertion of the guidewire, the inserting resistance is mainly caused by piercing the vessel, friction of the vessel wall, and blood viscosity [14], [22]. During the operation, the surgeons tentatively insert the guidewire by controlling the grasping force according to the current vascular environment and surgical experience. When the inserting force increases suddenly, the guidewire will slide passively between the fingers to cutoff excessive inserting force in real-time. The sliding of the guidewire between the fingers is called "passive sliding." The cutoff of excessive inserting force is defined as passive safety operation because it relies on the passive friction physical law to realize real-time inserting suspension. Then the tactile sense of the hand perceives this state, and after processing by the brain, the surgeon actively reduces the grasping forces or withdraws the guidewire. It is defined as an active safety operation. Because the blood vessels in the human body are tortuous and complicated, and each person's vessels are specific, the grasping force that should be used in the current vascular environment requires surgeons to make multiple attempts and years of surgical experience [23]. The real-time performance of the latter will be worse than that of the former because it requires tactile feedback and processing by the human brain.

The contributions of this article are as follows.

1) A series elastic actuator (SEA)-based guidewire manipulator is improved to realize remote force–position control of the guidewire and avoid the X-ray radiation of surgeons. And a multifunctional finger pulp mechanism is designed to measure the inserting force and perceive the grasping state of the guidewire simultaneously.
2) An orthogonal force coupling model based on the molecular–mechanical friction theory is designed to demonstrate the friction mechanism of cylindrical surgical instruments grasped by elastic grasping surfaces. It proved a relatively stable positive correlation coupling relationship between the grasping force and the inserting force threshold.
3) Imitating the safety operation of surgeons, a passive safety method is proposed to adjust the grasping force autonomously, which can satisfy the inserting force requirements of the phase delivery task and control the safety threshold suitable for the current environment. The experimental results demonstrate that the designed manipulator can grasp, twist, and insert the guidewire accurately, and the proposed method can effectively suppress the dangerous behavior of operators in real-time.

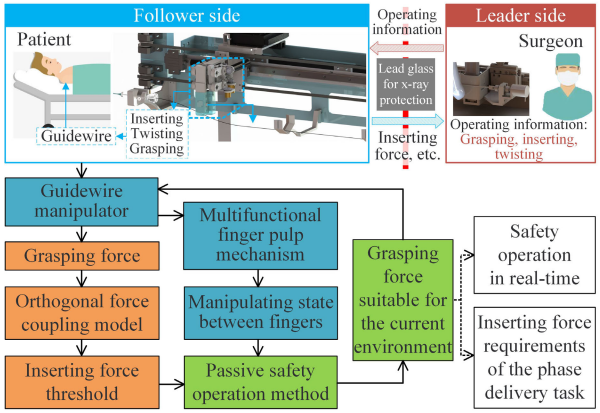

Fig. 1. Schematic of the proposed robot-assisted system for VIS.

The remainder of this article is organized as follows. First, the improved guidewire manipulator is conceived and developed in Section II. The orthogonal force coupling model is described in Section III, and Section IV presents the passive safety operation method. Then, experimental validations and analyses are carried out in Section V. Finally, discussions are made in Section VI. Section VII concludes this article.

II. Robotic System Developed

The schematic of the proposed robot-assisted VIS system with the passive safety method is shown in Fig. 1. The leader–follower operating architecture enables surgeons to avoid X-ray radiation during operations. The developed guidewire manipulator at the follower side can map the surgeons' operation at the leader side and complete the grasping, inserting, and twisting of the instruments. To enhance the safety of remote surgery, a passive safety method is designed based on the grasping state of the guidewire between the manipulator's fingers. Based on the inherent grasping force and the friction coupling mechanism of the grasped instruments, the safety threshold of the inserting force is adaptively adjusted to complete the operation and enhance safety.

The PG2 gripper is a parallel gripper based on two overlapped parallelogram mechanisms and an SEA, which can adjust the grasping force and operate objects between two fingers [24], [25]. The parallel grippers are suitable for grasping thinner objects. The gripper has only two actuators, but it can perform multiple manipulations with the help of highly overlapping motion spaces. The above features make the PG2 gripper potentially operate small guidewires (0.2–0.8-mm diameter) and catheters (1.3–2.3-mm diameter)

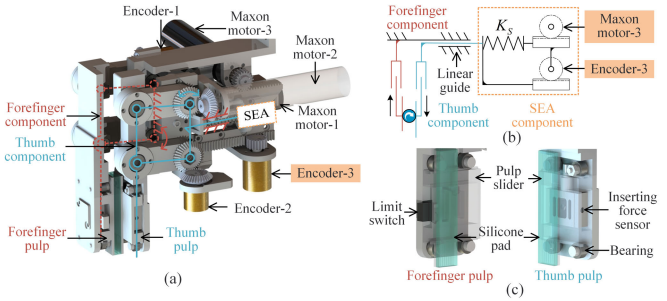

Fig. 2. Guidewire manipulator. (a) Detailed assembly. (b) Mechanism schematic. (c) Finger pulp mechanism.

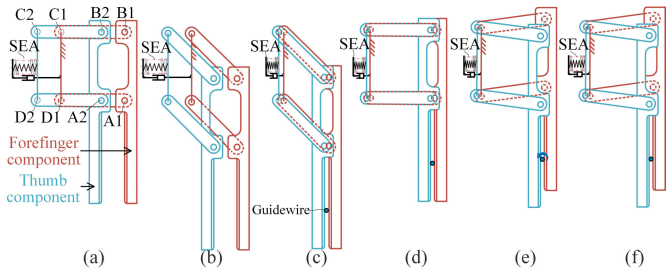

Fig. 3. Different operational states of the guidewire manipulator. (a) Opening. (b) Reaching. (c) Grasping. (d) Retracting. (e) Twisting. (f) Adjusting the grasping force.

in VIS. However, the previous PG2 gripper has a dead zone in the motion space under the desired grasping force, making the effective motion space only half [25]. Therefore, an actuator is added to decouple the grasping force control from the twisting.

The improved guidewire manipulator comprises the forefinger, thumb, and SEA components, as shown in red, blue, and orange in Fig. 2, respectively. The forefinger component and thumb component are designed based on two congruent parallelogram mechanisms, driven by the Maxon motor-1 (EC-max 16, Maxon, Switzerland) and the Maxon motor-2 (EC-max 16, Maxon, Switzerland), respectively. The two fingers move in the opposite direction to twist the guidewire, as shown in Fig. 3(e), and move in the same direction to reach and retract, as shown in Fig. 3(b) and (d). These functions facilitate the adjustment of guidewire insertion angle and multidevices' switching.

As shown in Fig. 2(a) and (b), the grasping force is controlled by the SEA, which consists of a spring, a linear guide, two rack and pinion mechanisms, Encoder-3 (1505, RoboBrain, China), and the Maxon motor-3 (EC-max 16, Maxon, Switzerland). The spring compression is measured by a 15-bit Encoder-3 and converted into force through a rack and pinion mechanism. The PG2 gripper is installed horizontally to decouple the gravity of the parts. Therefore, the force measured by the SEA is equal to the grasping force. The spring compression is adjusted by the Maxon motor-3 through a rack and pinion mechanism, thereby a grasping force closed loop is formed. The opening of the gripper is also driven by the Maxon motor-3. The grasping force can be calculated by

$$F_{\text{gsp}}(t) = (\theta_{\text{en}}(t) - \theta_{\text{en}}(0)) \cdot r_{\text{en}} \cdot K_s \tag{1}$$

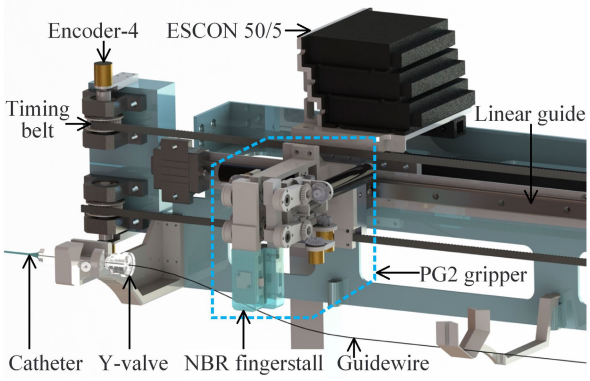

Fig. 4. Follower side of the VIS system.

where $F_{\text{gsp}}(t)$ represents the grasping force at time t, $\theta_{\text{en}}(t)$ represents the rotation angle of Encoder-3 at time t, r_{en} represents the reference circle radius of the gear installed on encoder-3, and K_s represents the spring coefficient of the SEA.

As shown in Fig. 2(c), the fingers' pulps are designed as sliders, which have tracks that fit tangentially with the bearings on the fingers and can slide freely along the inserting direction of the guidewire. A limit switch is installed on the forefinger to perceive the sliding state of the guidewire between the fingers. When the guidewire slides, the slider of the forefinger will trigger the limit switch, and then the sliding signal is obtained. It should be noted that the inserting force of the guidewire is only provided by the friction between the thumb and the guidewire because of the free sliding forefinger pulp. Therefore, an insertion force sensor (SBT630-19.6N, SIMBATOUCH, China) is embedded in the thumb pulp to measure the inserting force. Along the direction of the tracks, one end of the sensor is connected to the finger, and the other is connected to the slider. The working surface of the two fingers is silicone (shore hardness: 30 A, thickness: 2 mm).

The follower side of the VIS robot is shown in Fig. 4. It is mainly composed of a PG2 gripper, a push–pull mechanism, a catheter, a guidewire, a Y-valve, and an electrical system. The PG2 is installed on the linear sliding block of the push–pull mechanism and is firmly connected with a timing belt driven by a Maxon motor. The motion range of PG2 is kept within a certain distance from the Y-valve to avoid bending the flexible guidewire during insertion. The inserting force sensor and the SEA, respectively, measure the guidewire inserting force and grasping force.

The two fingers are covered with disposable gloves before the operation to ensure aseptic operation, as shown in Fig. 4. The glove is a disposable medical glove made of nitrile butadiene rubber (NBR) with a thickness of 0.08 mm. Its cross-sectional circumference is slightly larger than the fingers' to reduce the impact on the accuracy of the inserting force. Except for standard interventional devices, the guidewire is only in contact with medical gloves to ensure the asepsis during robot-assisted surgery. And the complex finger parts are wrapped in gloves to prevent debris of structural wear from entering the surgical system. Disposable gloves are removed after the operation, and it is unnecessary or simple to disinfect the gripper.

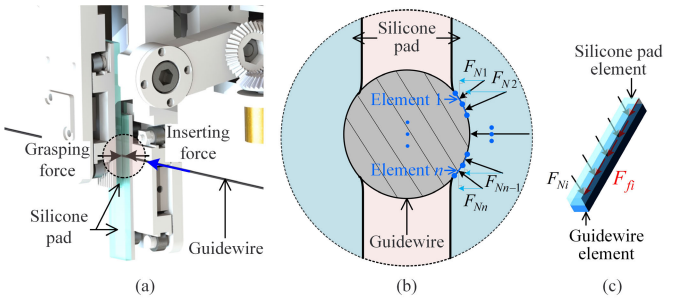

Fig. 5. Force analysis of elastic contact between the guidewire and silicone surface. (a) Gripper manipulates the guidewire. (b) Force analysis of the grasped guidewire. (c) Force analysis of contact elements.

III. Orthogonal Force Coupling Model

Based on the Coulomb friction law, the maximum static friction between two objects is related to the surface friction coefficient and normal load, which is slightly greater than the sliding friction force. Objects are not rigid bodies, the contact area changes with the normal load, and then the maximum static and sliding friction will change. For PG2 gripper, it is assumed that the grasping force is coupled with the maximum inserting force it provides. An orthogonal force friction model based on the molecular–mechanical friction theory is proposed to obtain the coupling relationship. The molecular–mechanical friction theory can be applied to analyze the dry friction of elastic materials such as silicone rubber [26]. The theory proved that friction is the sum of resistance generated by molecular and mechanical actions on the contact area. The contact friction can be expressed as

$$F_f = \alpha A_r + \beta F_N \tag{2}$$

where F_f represents the contact friction, α is a parameter related to the molecular properties of the surface, β is a parameter related to the mechanical properties of the surface, A_r represents the contact area, $A_r = A_{\text{mol}} + A_{\text{mech}}$, and F_N represents the external load. A_{mol} represents the contact area of molecular action, and A_{mech} represents the contact area of mechanical action.

As shown in Fig. 5(a), the guidewire is grasped and inserted, and it is mainly exerted by PG2 with radial grasping force and axial inserting force. The rubber glove is very thin, so the elastic contact model is built between the silicone pad and the guidewire without considering the glove's effect. The partially enlarged axial view of the guidewire is shown in Fig. 5(b). Since the hardness of the guidewire is much greater than that of the silicone pad, it is assumed that the former is a rigid body and the latter is an elastic body. When the grasping force is applied, the silicone pad will elastically deform and the contact area will change with the grasping force.

As shown in Fig. 5(c), since the force on the contact surface changes along the circumference of the guidewire section, the contact surface is microelemented, that is, the cylindrical arc surface is differentiated into rectangles with a large aspect ratio. Each microelement is assumed to be uniformly distributed, with no deformation at the edges and a flat contact surface. Based on the molecular–mechanical friction theory, the actual contact area of two elements in planar elastic contact can be approximately expressed as

$$A_{ri} = \left(\frac{A_{ci} \cdot \gamma \cdot F_{Ni}^2}{C_1 E^2 R_a}\right)^{\frac{1}{3}} \tag{3}$$

where A_{ci} represents the real contact area of two elements, γ represents the roughness radius, F_{Ni} represents the normal load on elements, E represents the material elastic modulus, R_a represents the roughness mean square error, and C_1 is a constant. Put (3) into the friction binomial (2) to obtain the relationship between two elastic contact elements sliding friction and normal load

$$F_{fi} = \alpha\left(\frac{A_{ci} \cdot \gamma \cdot F_{Ni}^2}{C_1 E^2 R_a}\right)^{\frac{1}{3}} + \beta F_{Ni} \tag{4}$$

where F_{fi} represents the sliding friction between microelements. Then the total sliding friction F_f between the guidewire and the unilateral grasping surface can be expressed as

$$F_f = \alpha \cdot \left(\frac{\gamma}{C_1 E^2 R_a}\right)^{\frac{1}{3}} \cdot \left[\sum_{i=1}^{n}\left(A_{ci}^{\frac{1}{3}} \cdot F_{Ni}^{\frac{2}{3}}\right)\right] + \beta \cdot \sum_{i=1}^{n} F_{Ni} \tag{5}$$

where n represents the total microelements, and A_{ci}, F_{Ni}, and n are parameters related to the grasping force. Then the orthogonal force coupling model can be expressed as

$$F_f = \left[\alpha \cdot \left(\frac{\gamma}{C_1 E^2 R_a}\right)^{\frac{1}{3}} \beta\right] \cdot P(F_N). \tag{6}$$

$P(F_N)$ is a vector related to F_N and can be expressed as

$$P(F_N) = \begin{bmatrix} y_1(F_N) \\ y_2(F_N) \end{bmatrix}$$

where $y_1(F_N) = \sum_{i=1}^{n}(A_{ci}^{(1/3)} \cdot F_{Ni}^{(2/3)})$, $y_2(F_N) = \sum_{i=1}^{n} F_{Ni}$.

The modeling and simulation of the relationship between the grasping force and the elastic contact deformation of the gripper working surface were performed. The rubber-like nonlinear materials can be approximated by a two-parameter Mooney–Rivlin model when the compressive strain is within 30%. The model is established based on phenomenology and two assumptions as: 1) the rubber material is isotropic and has volume incompressibility and 2) Hooke's law is followed in the shear deformation, that is, the stress–strain relationship is linear. The two-parameter Mooney–Rivlin constitutive model of an isotropic incompressible material can be expressed as

$$W = C_{10}(I_1 - 3) + C_{01}(I_2 - 3) \tag{7}$$

where W represents the strain energy density, C_{10} and C_{01} are the Rivlin coefficients, and I_1 and I_2 are the first and second stress invariants, respectively. The relationship between the principal stress t_i and the principal elongation ratio λ_i of a rubber material is

$$t_i = 2\left(\lambda_i^2 \frac{\partial W}{\partial I_1} + \frac{1}{\lambda_i^2}\frac{\partial W}{\partial I_2}\right) + p \tag{8}$$

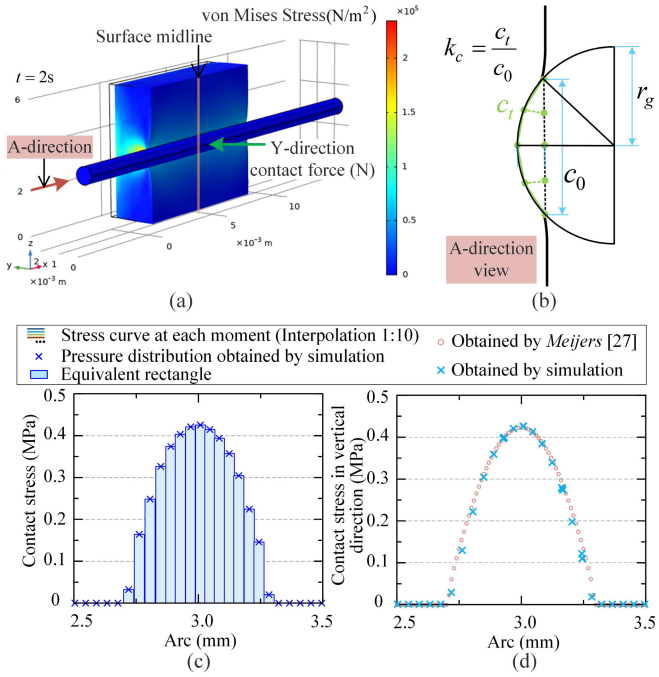

Fig. 6. Elastic contact model simulation results. (a) State when the silicone pad is deformed by 0.3 mm. (b) A-direction view in (a). (c) Pressure distribution in the surface midline at the simulation time of 1.75 s (indenter displacement: 2.625 mm). (d) Comparison of the simulated pressure distribution with that obtained by Meijers [27].

where p represents the hydrostatic pressure, $i \in \{1, 2, 3\}$. The three principal stress differences are obtained by subtracting the principal stresses in each direction from (8)

$$t_i - t_j = 2\left(\lambda_i^2 - \lambda_j^2\right)\left(\frac{\partial W}{\partial I_i} + \lambda_k^2 \frac{\partial W}{\partial I_j}\right) \tag{9}$$

where $i, j, k \in \{1, 2, 3\}$. In the case of uniaxial tension, $t_2 = t_3 = 0$, and $\lambda_2^2 = \lambda_3^2 = \lambda_1^{-1}$. Therefore, the strain–stress relationship of a uniaxial tensile test specimen can be expressed as

$$\sigma_{11} = 2\left(\lambda_1^2 - \frac{1}{\lambda_1}\right)\left(\frac{\partial W}{\partial I_1} + \frac{1}{\lambda_1}\frac{\partial W}{\partial I_2}\right). \tag{10}$$

After calculating the partial derivative of (7) and substituting the results into (10)

$$\sigma_{11} = 2\left(\lambda_1^2 - \frac{1}{\lambda_1}\right)\left(C_{10} + \frac{1}{\lambda_1}C_{01}\right) \tag{11}$$

where σ_{11} represents the Cauchy stress, $\sigma_{11} = (F/A_0)$, F represents the principal stress direction load, and A_0 represents the original cross-sectional area of the specimen. After testing the sample and fitting (11) by the least-square method, the two parameters were obtained, that is, $C_{10} = 21\,894$ Pa and $C_{01} = 96\,474$ Pa.

The elastic contact model between the guidewire and the silicone pad was simulated. The contact state of the two working surfaces of the gripper was assumed to be the same, and only the loading position was different. Therefore, to reduce the number of meshes, only the state of the unilateral contact surface was simulated and the length of the silicone pad was reduced to 6 mm, as shown in Fig. 6(a). In the simulation, the guidewire gradually deforms the silicone pad along the

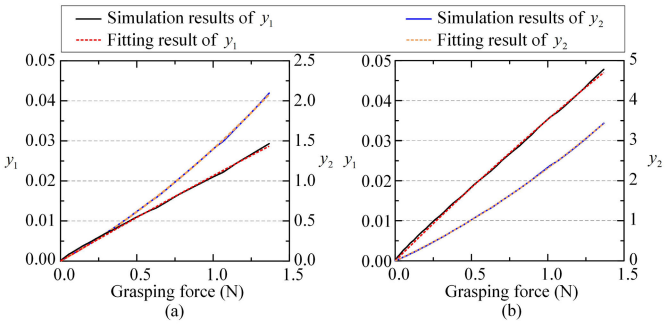

Fig. 7. Curves of y_1 and y_2 with the grasping force. (a) Guidewire. (b) Catheter.

Y-axis direction, the total pressing amount is 0.3 mm, and the simulation step size is 1.5×10^{-3} mm. Fig. 6(a) shows the state when the silicone pad is deformed by 0.3 mm. The pressure distribution in the surface midline at the simulation time of 1.75 s is shown in Fig. 6(d). The simulated pressure distribution on the contact surface matches well with that obtained by Meijers [27] (Pearson correlations = 0.998 and significant level: 0.05). Based on the midpoint rule, the stress state near the nodes was replaced by rectangles approximately, as shown in the histogram in Fig. 6(c). The distance between each surface mesh nodes of the silicone pad was elongated in the extrusion, as shown in Fig. 6(b). Then the contact area between the guidewire and the silicone pad changed. The elastic surface elongation can be written as

$$k_c = \frac{c_t}{c_0} \tag{12}$$

where k_c represents the elongation of the contact border in the section, c_0 represents the maximum distance of the contact border, which can be obtained by simulation, c_t represents the length of the contact border at time t, $c_t = 2r_g \cdot \arcsin(c_0/r_g)$, and r_g represents the radius of the guidewire. Then k_c can be expressed as

$$k_c = \frac{2r_g \cdot \arcsin\left(\frac{c_0}{2r_g}\right)}{c_0}. \tag{13}$$

The elements in $P(F_N)$ can be written as

$$\sum_{i=1}^{n}\left(A_{ci}\sigma_{Ni}^{\frac{2}{3}}\right) = \sum_{i=1}^{n}\left(\frac{(x_i - x_{i-1}) + (x_{i+1} - x_i)}{2} d_s k_c \sigma_{Ni}^{\frac{2}{3}}\right) \tag{14}$$

$$\sum_{i=1}^{n}\left(A_{ci}\sigma_{Ni}\right) = \sum_{i=1}^{n}\left(\frac{(x_i - x_{i-1}) + (x_{i+1} - x_i)}{2} d_s k_c \sigma_{Ni}\right) \tag{15}$$

where σ_{Ni} represents the ith node stress in the contact border, and $F_{Ni} = A_{ci}\sigma_{Ni}$. x_i represents the ith node position, especially $x_0 = x_1$, and $x_{n+1} = x_n$. d_s represents the width of the silicone pad, and $d_s = 7.5$ mm.

1) Guidewire: Based on the simulation results, the curves of y_1 and y_2 with the grasping force were calculated and drawn, as shown in the black and blue solid lines in Fig. 7(a), respectively. Two elements were obtained by polynomial fitting and

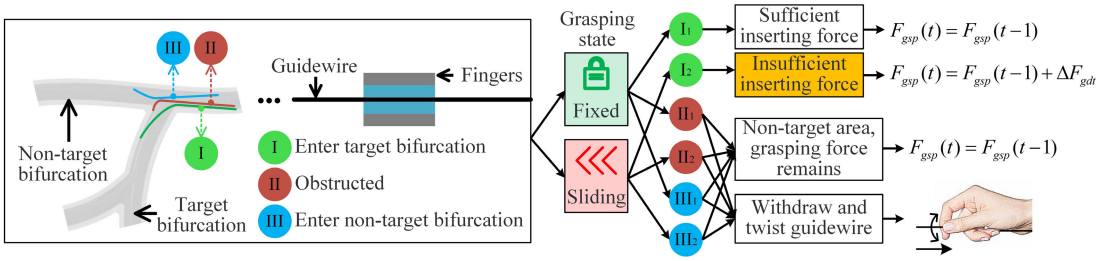

Fig. 8. Passive safe operation strategy. Where $F_{\mathrm{gsp}}(t)$ represents the grasping force at time t, and ΔF_{gdt} represents the gradient of force adjustment.

written as

$$\begin{cases} y_1 = -0.0009F_N^2 + 0.0222F_N \\ y_2 = 0.3359F_N^2 + 1.062F_N. \end{cases} \tag{16}$$

The two fitting curves are shown in red and orange dotted lines in Fig. 7(a), and their coefficients of determination are $R_1^2 = 0.999$ and $R_2^2 = 0.9999$, respectively. Substituting (16) into (6) to obtain the guidewire orthogonal force coupling model

$$F_f = \begin{bmatrix} a_{gw} & b_{gw} \end{bmatrix} \begin{bmatrix} -0.0009F_N^2 + 0.0222F_N \\ 0.3359F_N^2 + 1.062 \cdot F_N \end{bmatrix}. \tag{17}$$

For a certain contact model, a_{gw} and b_{gw} are constants.

2) Catheter: Similarly, the two elements of the catheter orthogonal force coupling model can be expressed as

$$\begin{cases} y_3 = -0.0025F_N^2 + 0.0378F_N \\ y_4 = 0.5431F_N^2 + 1.7672F_N. \end{cases} \tag{18}$$

The two fitting curves are shown in red and orange dotted lines in Fig. 7(b), and their coefficients of determination are ${R_1}^2 = 0.999$ and ${R_2}^2 = 1$, respectively. Substituting (18) into (6) to obtain the catheter orthogonal force coupling model

$$F_f = \begin{bmatrix} a_{ct} & b_{ct} \end{bmatrix} \begin{bmatrix} -0.0025F_N^2 + 0.0378F_N \\ 0.5431F_N^2 + 1.7672F_N \end{bmatrix} \tag{19}$$

where a_{ct} and b_{ct} are constants.

IV. Passive Safety Method

Many factors affect the inserting resistance of the guidewire in blood vessels because there exists considerable variability among the different blood vessels. It is difficult to model and predict the resistance [14]. This is one of the unsolved research problems that hinder even the existing active safety methods. In operation, surgeons tentatively insert guidewires at key locations such as vascular branches, tortuous places, and lesions. The initial grasping force is applied based on the surgeons' experience rather than a large grasping force to fix the guidewire. It indicates that the current maximum inserting force cannot complete the task if the guidewire passively slides between the fingers and is not obstructed. Then the surgeon will slightly increase the grasping force, which will increase the maximum inserting force threshold, and try again. The surgeons continuously perceive the minimum grasping force required by the current vascular environment through the operation method, which enables safety insertion by avoiding sudden, unsuitable inserting force. Therefore, a passive safety method for robot-assisted surgery is designed to imitate the tentative guidewire insertion of surgeons' hands, as shown in Fig. 8.

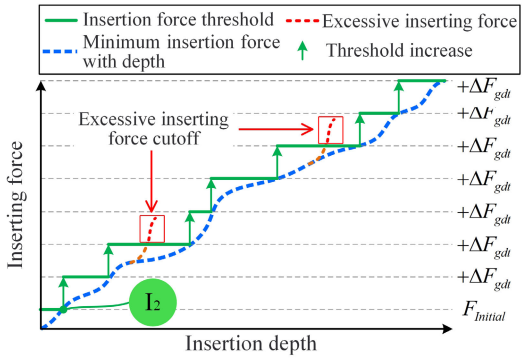

Fig. 9. Expected effects of the passive safety operation strategy.

Based on the orthogonal force coupling model, we can control the maximum inserting force by controlling the grasping force of the gripper. Imitating surgeons' operation, the grasping force is initially set to a low level because the robot does not yet have the surgeons' experience, and then tentatively inserts the guidewire. As shown in Fig. 8, the guidewire inserting states are divided into three types in the blood vessel: entering the target bifurcation, obstructed, and entering the nontarget bifurcation. The operators observe and judge the current state through the real-time images. The three insertion states include two grasping states, respectively: fixed and sliding.

1) Guidewire Enters the Target Bifurcation: If the guidewire slides between the fingers, it is considered that the inserting force threshold provided by the grasping force is not enough to complete the current delivery task. So the grasping force needs to be increased. If the guidewire does not slide, the inserting state is considered normal and the grasping force remains.

2) Guidewire Is Obstructed or Enters Nontarget Bifurcation: The guidewire is operated in a nontarget area, regardless of sliding, the grasping force remains, and the guidewire is retracted and twisted.

As shown in Fig. 9, the blue dotted line represents the curve of minimum insertion force with the insertion depth, which has a certain randomness and is difficult to predict according to the environment accurately. The designed passive safety method adjusts the grasping force autonomously by identifying the sliding state of the guidewire under the I_2 state, as shown by the green arrow and line in Fig. 9. The adjusted grasping force

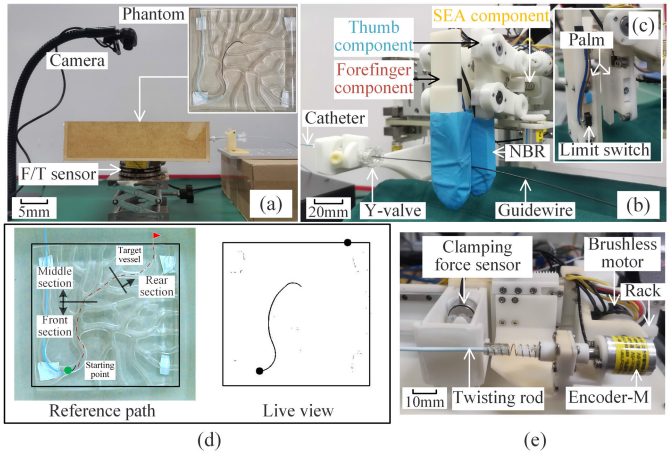

Fig. 10. Experimental setups for evaluation. (a) Phantom. (b) Follower side. (c) Structure of finger pulp. (d) Operator view. (e) Leader-side manipulator.

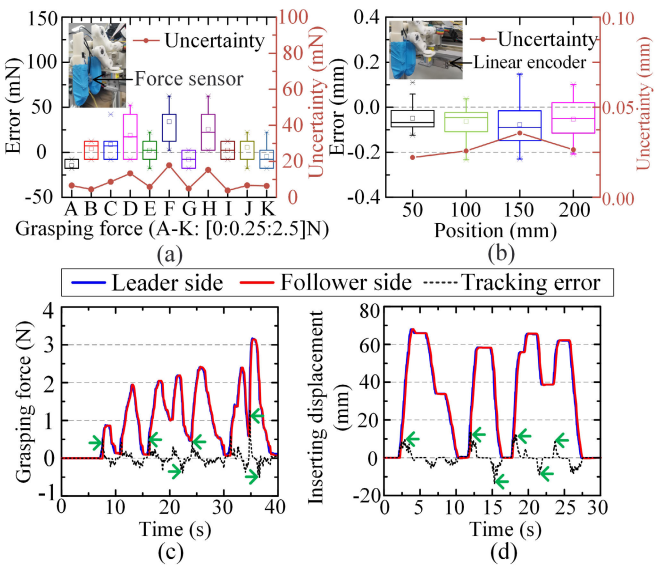

Fig. 11. Performance evaluation of the VIS robot system. (a) Grasping force accuracy evaluation. (b) Linear motion positioning accuracy evaluation. Performance evaluation of leader–follower (c) grasping force tracking and (d) inserting displacement tracking.

can not only complete the current delivery task but also cut off the increase in the inserting force passively in real-time, avoiding excessive the contact force between the guidewire and the vessel wall shown by the red dotted lines. Therefore, the passive safety method solves two difficulties in the existing active safety methods as follows.

1) The problem of setting insertion force thresholds for different insertion depths and vessel conditions.
2) The problem of inevitable delay in safety methods response caused by large amounts of real-time data collection, processing, and algorithm calculations.

V. Evaluation and Experiments

A. Experimental Setup

The experimental setup consists of a follower side and a leader side, as shown in Fig. 10(a)–(e), respectively. As shown in Fig. 10(a), the catheter was preinserted into the coronary artery inlet of the phantom (glass material filled with a liquid containing biosurfactant). The guidewire passed through the Y-valve, the catheter, and was grasped, twisted, and inserted into the coronary artery of the phantom by the gripper. The phantom was connected to the top of the F/T sensor (ATI Industrial Automation, USA) so as to measure the force applied by the guidewire on the vessel wall. It is difficult to measure the contact force accurately. The whole body composed of the vessel model and the guidewire inserting part, which is supported by the force sensor and the inserting force from the guidewire at the entrance of the phantom, can be easily measured. The measured force can represent the contact force during the insertion process of instruments to an extent [16]. The images of the guidewire were taken by a camera, processed by binarization, and then transmitted to the leader side, as shown in Fig. 10(d). The phantom was divided into three sections according to the reference path depth: front section, middle section, and rear section. As shown in Fig. 10(c), a limit switch was installed on the forefinger pulp to detect the sliding of the guidewire, and the inserting force sensor was embedded on the thumb pulp to measure the insertion force. The grasping force was measured by the SEA component and a grasping force closed loop was established.

The leader-side view is shown in Fig. 10(d), which includes a static reference path and a live view of the guidewire. The operator can only see the guidewire outline through the latter, consistent with the surgeons' view under X-ray. The leader manipulator is shown in Fig. 10(e). Encoder-M (1505, RoboBrain, China) was used to measure the twist angle of the operator. The delivery displacement was measured by a magnetic encoder on the brushless motor through the rack and pinion transmission. The leader-side grasping force was measured by a clamping force sensor (SBT674-19.6N, SIMBATOUCH, China). Then, the operation information, collected by the leader side, was transmitted to the follower side to realize the leader–follower mapping control.

B. Performance Evaluation of the VIS Robot

First, the grasping force control accuracy and the linear motion positioning accuracy of the guidewire manipulator were evaluated by repeated experiments.

1) Grasping Force Accuracy Evaluation: The grasping force of the manipulator was repeatedly controlled six times at 0–2.5 N (gradient: 0.25 N) and collected by the pressure sensor (SBT674-19.6N, resolution: 20 mN, SIMBATOUCH, China). The force error and uncertainty are shown in Fig. 11(a). The mean absolute error (MAE) of the grasping force control is 16.01 mN, and the root mean square error (RMSE) is 21.6 mN.

2) Linear Motion Positioning Accuracy Evaluation: Repeat positioning 15 times at 50, 100, 150, and 200 mm in the motion stroke respectively. The absolute position was collected with a linear scale (JCXE-DK, resolution: 5 μm, FOIC, China). The positioning error and uncertainty of each point are shown in Fig. 11(b). The repeated positioning

accuracy of each point is ±0.117, ±0.136, ±0.188, and ±0.154 mm, respectively. And MAE = 0.0848 mm and RMSE = 0.1034 mm.

Leader–follower force and position control performance is important for robot-assisted teleoperation VIS. Due to the improvement of the mechanism and motion control, the leader–follower grasping force tracking performance and position tracking performance were reevaluated.

3) Performance Evaluation of Leader–Follower Grasping Force Tracking: In the previous experiment, the SEA component was calibrated [24], and the spring coefficient of the SEA is 1.122 N/mm. In the evaluation experiment, the operator randomly applied the grasping force on the leader side. The tracking curves of the leader–follower grasping force are shown in Fig. 11(c). After taking the absolute values of the errors at all times, the average absolute error was 52.72 mN, and the average relative error was 5.55%.

4) Performance Evaluation of Leader–Follower Inserting Displacement Tracking: In the evaluation experiment, the operator randomly pushed and pulled multiple times at the leader side. The leader–follower inserting displacement tracking curves are shown in Fig. 11(d). After taking the absolute values of the errors at all times, the average absolute error was 2.12 mm, and the average relative error was 6.42%. In the previous experiment, the leader–follower average twisting angle tracking accuracy was 0.1784 mm, and the relative error was 3.04% [24]. The tracking errors pointed out by the green arrows in Fig. 11(c) and (d) were large because of the leader–follower response delay and the large operating speed of the leader side. However, the errors were decreased to a low level within 0.31 s.

C. Parameters' Identification of the Orthogonal Force Coupling Model

In this section, the constants in (17) and (19) were identified experimentally to prove the stable coupling relationship between the grasping and the maximum inserting force. The guidewire was fixed with a Y-valve and grasped by the gripper in the experiment. Then the gripper was controlled to move at a constant speed under the target grasping force. The friction between the guidewire and the thumb finger was measured by the inserting force sensor, as shown in Fig. 10(b). The target grasping force was set to 0.05 and 0.1–2.5 N with a gradient of 0.1 N.

The data of the stable sliding area of the guidewire and catheter in the experiment under each grasping force are shown in the box plot of Fig. 12. It can be seen that the grasping force was positively correlated with the sliding friction. The average value of the sliding friction force under different amount of grasping was considered to represent the current friction force, and the sliding friction curve was shown by the black line in Fig. 12. Then the parameters in the orthogonal force coupling model were obtained by least-squares fitting, as shown in Table I. Where c was the compensation intercept, which was used to compensate for the step characteristic of sliding friction when the grasping force was close to 0. The fitting curves and their uncertainties are shown in the red lines and dark red lines in Fig. 12, respectively. The maximum

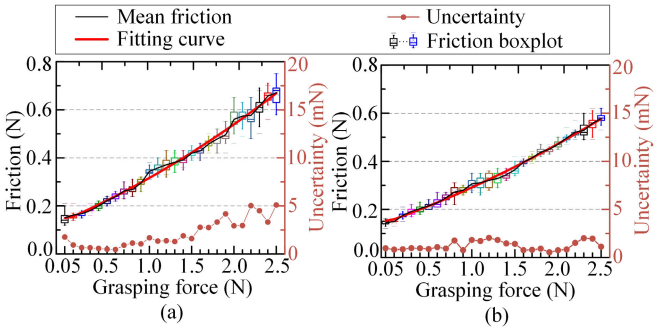

Fig. 12. Relationship between the friction force and the grasping force of instruments. (a) Guidewire. (b) Catheter.

TABLE I
ORTHOGONAL FORCE COUPLED MODEL FITTING PARAMETERS FOR CATHETER AND GUIDEWIRE

Parameters	a	b	c	Coefficients of determination	Maximum uncertainty
Guidewire	1.4038	0.1088	0.1416	0.9941	5.47mN
Catheter	1.4664	0.0402	0.1464	0.9965	2.08mN

uncertainty of the guidewire is 5.47 mN and that of the catheter is 2.08 mN. The coefficients of determination between the fitting curves and the experimental results were 0.9941 and 0.9965, respectively. Therefore, the designed orthogonal force coupling model can explain the coupling relationship between the maximum inserting force and the grasping force. Furthermore, it also proved a relatively stable positive correlation coupling relationship between the two forces, which was the key to realize the passive safety method.

D. Evaluation of the Passive Safety Method

In vitro experiments were performed to evaluate the feasibility of the passive safety method. The operator operated the VIS robot based on the operator view to insert the guidewire from the starting point to the target point, as shown in Fig. 10(d). The guidewire needed to pass by seven bifurcations to reach the target point. The operator inserted the guidewire tentatively with as little contact force as possible. The experiment was divided into an experimental group and a control group. The former turned on the passive safety method, and the latter turned it off and only had the position control. The initial grasping force of the experimental group was 0.25 N, and the increasing gradient was 0.25 N. The grasping force of the control group was set at a constant 2 N. Five experiments were performed, and the results are shown in Table II. The maximum contact force of the experimental group was obviously smaller than that of the control group in the front and middle sections. Compared with the control group, the maximum contact force of the experimental group was reduced by 41.54% and 40.29% in the front and middle sections, respectively. The reason is that the control group appeared larger contact force in the front and middle sections, which were even larger than that in the deeper rear section. However, the maximum contact force of the experimental group increased gradually with the insertion depth and was relatively low. The maximum contact

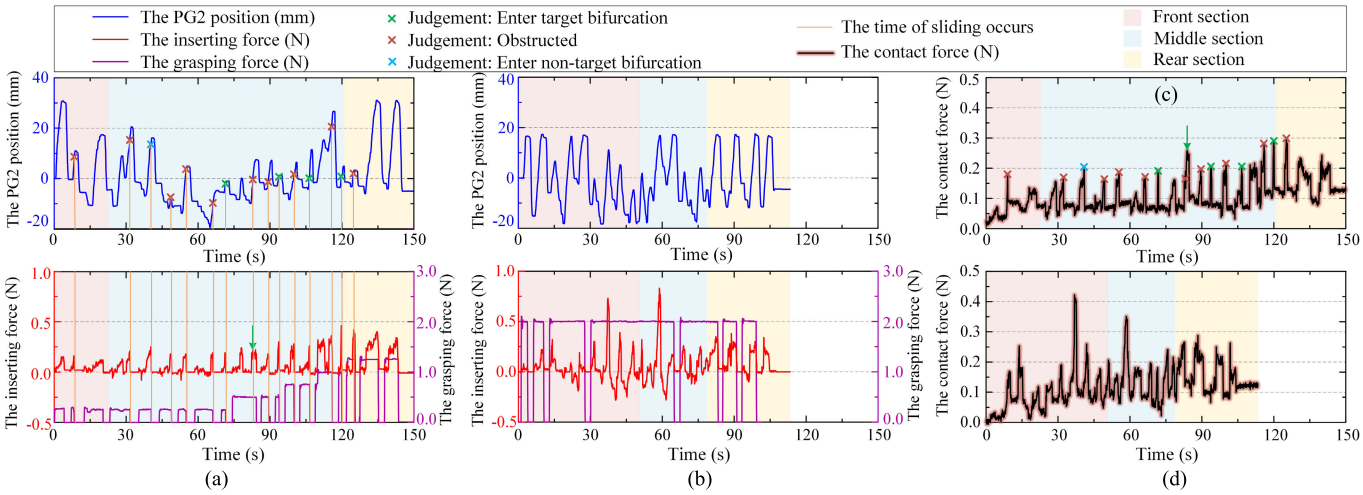

Fig. 13. Evaluation results of the passive safety method. (a) Results of the experimental group. (b) Results of the control group. (c) Contact force between the guidewire and the phantom in the experimental group. (d) Contact force in the control group.

TABLE II
MAXIMUM CONTACT FORCE AT EACH SECTION IN THE FIVE SETS OF EXPERIMENTS

NO.	Experimental group (N)			Control group (N)		
	Front	Middle	Rear	Front	Middle	Rear
1	0.134	0.169	0.250	0.234	0.234	0.259
2	0.144	0.191	0.278	0.209	0.419	0.172
3	0.138	0.197	0.225	0.194	0.313	0.231
4	0.166	0.209	0.284	0.247	0.416	0.281
5	0.178	0.262	0.300	0.416	0.344	0.281
Average	**0.152**	**0.206**	0.268	0.260	0.345	0.245

TABLE III
EXPERIMENTAL RESULTS OF THE FIFTH GROUP

		Experimental group	Control group
Tentative insertion number		22	17
Maximum inserting force (N)	Front section	0.160	0.720
	Middle section	0.290	0.810
	Rear section	0.450	0.380
Maximum contact force (N)	Front section	0.178	0.416
	Middle section	0.262	0.344
	Rear section	0.300	0.281
Completion time (s)		150	114

force of the two groups was basically the same in the rear section.

The fifth experiment was singled for detailed analysis, and the experimental results are shown in Fig. 13 and Table III. As shown by the blue lines in Fig. 13, the experimental group completed 22 insertion attempts and 17 in the control group. Among them, the sliding state of the guidewire occurred 15 times in the experimental group, as shown by the orange line and crosses in Fig. 13(a). Among them, the operator judged the insertion state: four times in state I, ten times in state II, and one time in state III. When state I occurred, it was considered that the maximum inserting force provided by the current grasping force could not satisfy the task requirements. Therefore, the grasping force was automatically increased by 0.25 N in the next attempt to increase the inserting force threshold, as shown by the purple line in Fig. 13(a). When states II and III occurred, the grasping force remained unchanged for the next attempt. The red line in Fig. 13(a) represented that the inserting force threshold increased from 0.13 to 0.41 N after four grasping force adjustments. On one hand, it showed that with the increase in the insertion depth, the insertion resistance and the required inserting force increased. On the other hand, it showed that the designed passive safety method could obtain the required suitable inserting force threshold in different vessel environments. Then the suitable grasping force was controlled autonomously so that the gripper inserted the guidewire tentatively within the suitable inserting force threshold. Under the grasping force, the follower side can not only complete the delivery task in the current environment but also prevent unsuitable inserting force surges in real-time. The experimental results of the control group are shown in Fig. 13(b). Compared with the experimental group, there were many times of large inserting forces and contact forces in the front and middle sections of the phantom. The reason was that obstructions occurred, but the insertion was not stopped in time.

As shown in Table III, the experimental group inserting force peaks gradually increased with the inserting depth. The inserting force peaks were much smaller than those of the control group in the front and middle sections. It indicated that the designed passive safety method can effectively reduce the contact force applied by the guidewire on the phantom under the premise of satisfying the requirements of the task. The completion time of the experimental group was 150 s, and the efficiency was lower than that of the control group whose completion time was 114 s. The reason was that when the guidewire slid, the gripper automatically opened and waited for the operator to judge the state before trying again. It was also demonstrated by the grasping force curves shown by the purple lines in Fig. 13. The green arrow in Fig. 13(c) showed that the contact force was still increasing after the sliding occurred, but the inserting force did not increase at the corresponding position in Fig. 13(a). It indicated that the gripper failed to open in time. When the forefinger pulp slid to the limit position, the inserting force of the guidewire was applied by the two fingers pulps at the same time, which caused

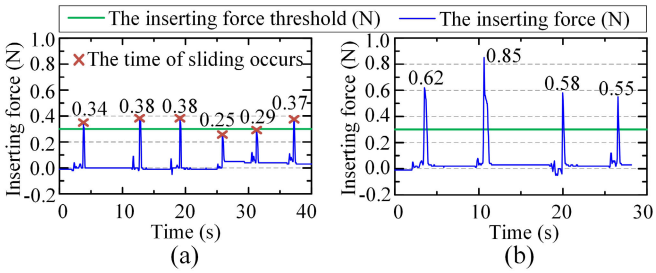

Fig. 14. Reliability experimental results. (a) Experimental group: the passive safety method. (b) Control group: the active safety method.

the proximal contact force to increase continuously. This problem caused by the guidewire sliding signal was repeatedly triggered due to rapid stepping of the flexible guidewire in the phantom. This problem can be solved by trigger debounce.

VI. Discussion

Sections II–V present the structure design, algorithm design, and experimental validation of the VIS robot system. Before the end of this article, we think that the following discussions are necessary to enhance comprehension.

A. On the Reliability of the Passive Safety Method

The experimental group turned on the passive safety method and set the inserting force threshold to 0.3 N based on the orthogonal force coupling model. The control group turned on the active safety method based on the inserting force threshold, and the threshold was set to 0.3 N. When the inserting force reached the threshold, the gripper released the guidewire. In the experiment, the proximal end of the guidewire was fixed, and the gripper stepped forward rapidly at a speed of 500 mm/s. The inserting force was measured in real-time by the inserting force sensor, as shown in Fig. 14.

The four experiments of the control group were all greater than the threshold, with an average absolute error of 0.35 N and a relative error of 117%. In the experimental group, the guidewire slid in time near the threshold, the average absolute error was 0.055 N, and the relative error was 18.3%. The results demonstrated that the designed algorithm is more reliable and real-time. The reason for the error in the experimental group is that the actual friction situation is complicated, and it can only control the approximate range. The reason for the large error in the control group is that when the system detected an inserting force greater than 0.3 N, the gripper did not release the guidewire in time and continued to inserting it. It resulted in the insertion force increasing continuously until the gripper released the guidewire after about 380 ms.

Even if the real-time performance of some robot-assisted surgical systems satisfies the requirements, predicting and setting suitable thresholds in the complex vascular environment remains difficult for the existing active safety methods, as shown in Table IV. The designed passive safety method can control the suitable inserting force threshold autonomously and reliably, which has the potential to improve the safety of robot-assisted remote surgery.

TABLE IV
Comparison of the Proposed Method With Existing Methods

Relevant efforts	The basis for the safety threshold	The gradient of the threshold	Intervention trigger process
Bao et al. [17]	Static distal force	3 (custom: 0.1, 1.4, 1.7N)	Trigger delay (Force collecting and program processing, etc.)
Shi et al. [18]	Dynamic features of distal force	Semi-adaptive (custom: trigger value=2)	
Jin et al. [19]	Static proximal force	1 (custom: 0.342N)	
This paper	Manipulating state between fingers	**Adaptive** (0-1.5N)	**Real-time (Non-program-based)**

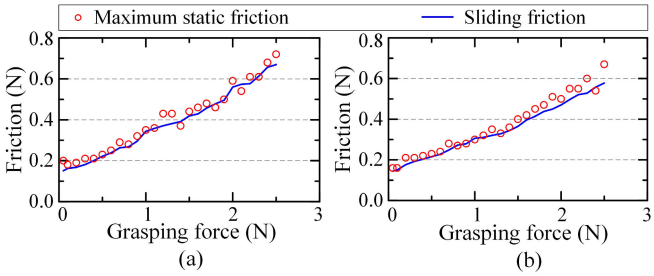

Fig. 15. Experimental results of maximum static friction and sliding friction. (a) Guidewire. (b) Catheter.

B. On the Reasons for Using Sliding Friction Instead of Maximum Static Friction When Modeling

When the guidewire state changes from relatively fixed to passive sliding between the fingers, the insertion resistance must exceed the maximum static friction. However, the orthogonal force coupling model is established by the relationship between the sliding friction and the grasping force. The reason is that it is difficult to build a model that accurately explains the maximum static friction due to many influencing factors. Therefore, based on the third law of Coulomb friction, we assumed that the maximum static friction is slightly greater than the sliding friction. The assumption was tested in the experiments. According to the experimental results in Section V-C, the friction results of the guidewire and catheter are shown in Fig. 15(a) and (b), respectively. The first peak of the inserting force under each grasping force was taken as the maximum static friction as shown by the red circles in Fig. 15. The average inserting force in the stable sliding area was taken as the sliding friction as shown by the blue lines in Fig. 15. The mean absolute error of the two forces was 23.8 mN (Pearson correlations = 0.990 and significant level: 0.05) for the guidewire and 23.5 mN (Pearson correlations = 0.989 and significant level: 0.05) for the catheter. It can be seen that the static friction is slightly greater than the sliding friction at most positions, which was consistent with the assumption. Furthermore, the proposed orthogonal force coupling model is not to obtain an accurate functional relationship, but to prove a relatively stable positive correlation between the two forces, so the assumption will not affect the outcome of the proposed methods.

VII. Conclusion

In this article, an SEA-based guidewire manipulator with adjustable grasping force function was improved, which can grasp, twist, and insert the guidewire. A two-fingered pulp component that can measure the inserting force and perceive the manipulating state of the guidewire simultaneously was designed. An orthogonal force coupling model based on the mechanical–molecular friction model was proposed to control the grasping state of the surgical instruments. The stable coupling relationship between the grasping force and the inserting force threshold of the cylindrical surgical instruments was proved through finite element simulation and experiments. Then, based on the coupling model, a passive safety method was proposed. By judging the inserting state when the guidewire slides, the inserting force threshold suitable for the current environment was adjusted autonomously. Finally, experiments were performed to validate the performance of the VIS robot and the effectiveness of the passive safety method. The experimental results demonstrated that the designed passive safety method can automatically and reliably adjust the grasping force according to the inserting state of the guidewire, effectively reducing the contact force with the vessels and ensuring the safety of the operation.

However, several limitations existed in this article. First, the inserting states of the instruments still need to be judged by the operator, which affects the efficiency of the operation. Second, the proposed method is not tested in vivo. In the future, more modalities of surgical information will be considered in the instrument state prediction. And we will validate the proposed method through in vivo experiments.

References

[1] *World Health Statistics 2021: Monitoring Health for the SDGs, Sustainable Development Goals*, World Health Org., Geneva, Switzerland, 2020.

[2] S. Zhang et al., "Design and characteristics of 3D magnetically steerable guidewire system for minimally invasive surgery," *IEEE Robot. Autom. Lett.*, vol. 7, no. 2, pp. 4040–4046, Apr. 2022.

[3] B. Rivkin et al., "Electronically integrated microcatheters based on self-assembling polymer films," *Sci. Adv.*, vol. 7, no. 51, 2021, Art. no. eabl5408.

[4] A. Hooshiar, A. Payami, J. Dargahi, and S. Najarian, "Magnetostriction-based force feedback for robot-assisted cardiovascular surgery using smart magnetorheological elastomers," *Mech. Syst. Signal Process.*, vol. 161, Dec. 2021, Art. no. 107918.

[5] V. Ramanathan, S. M. Almeida, and K. Fernando, "Occupational dose measurement for radiographers during cardiac catheterization procedures," *Int. J. Sci. Res. Publications*, vol. 11, no. 4, pp. 476–481, Apr. 2021.

[6] W. Duan et al., "Technical and clinical progress on robot-assisted endovascular interventions: A review," *Micromachines*, vol. 14, no. 1, p. 197, Jan. 2023.

[7] X. Bao, S. Guo, N. Xiao, Y. Li, C. Yang, and Y. Jiang, "A cooperation of catheters and guidewires-based novel remote-controlled vascular interventional robot," *Biomed. Microdevices*, vol. 20, no. 1, pp. 1–19, 2018.

[8] Y. Zhao et al., "A novel noncontact detection method of surgeon's operation for a master-slave endovascular surgery robot," *Med. Biol. Eng. Comput.*, vol. 58, no. 4, pp. 871–885, 2020.

[9] X. Yin, S. Guo, N. Xiao, T. Tamiya, H. Hirata, and H. Ishihara, "Safety operation consciousness realization of a MR fluids-based novel haptic interface for teleoperated catheter minimally invasive neurosurgery," *IEEE/ASME Trans. Mechatronics*, vol. 21, no. 2, pp. 1043–1054, Apr. 2015.

[10] X. Jin, S. Guo, J. Guo, P. Shi, T. Tamiya, and H. Hirata, "Development of a tactile sensing robot-assisted system for vascular interventional surgery," *IEEE Sensors J.*, vol. 21, no. 10, pp. 12284–12294, May 2021.

[11] A. Hooshiar, A. Sayadi, J. Dargahi, and S. Najarian, "Integral-free spatial orientation estimation method and wearable rotation measurement device for robot-assisted catheter intervention," *IEEE/ASME Trans. Mechatronics*, vol. 27, no. 2, pp. 766–776, Apr. 2021.

[12] R.-Q. Li et al., "A unified framework for multi-guidewire endpoint localization in fluoroscopy images," *IEEE Trans. Biomed. Eng.*, vol. 69, no. 4, pp. 1406–1416, Apr. 2021.

[13] S. Wang, Z. Liu, X. Shu, and L. Xie, "Mechanism design and force sensing of a novel cardiovascular interventional surgery robot," *Int. J. Med. Robot. Comput. Assist. Surg.*, vol. 18, no. 4, p. e2406, Aug. 2022.

[14] H.-S. Song, B.-J. Yi, J. Y. Won, and J. Woo, "Learning-based catheter and guidewire-driven autonomous vascular intervention robotic system for reduced repulsive force," *J. Comput. Des. Eng.*, vol. 9, no. 5, pp. 1549–1564, 2022.

[15] Y. Yan et al., "Machine learning-based surgical state perception and collaborative control for a vascular interventional robot," *IEEE Sensors J.*, vol. 22, no. 7, pp. 7106–7118, Apr. 2022.

[16] D. Wu et al., "Deep-learning-based compliant motion control of a pneumatically-driven robotic catheter," *IEEE Robot. Autom. Lett.*, vol. 7, no. 4, pp. 8853–8860, Oct. 2022.

[17] X. Bao et al., "Multilevel operation strategy of a vascular interventional robot system for surgical safety in teleoperation," *IEEE Trans. Robot.*, vol. 38, no. 4, pp. 2238–2250, Aug. 2022.

[18] P. Shi et al., "Design and evaluation of a haptic robot-assisted catheter operating system with collision protection function," *IEEE Sensors J.*, vol. 21, no. 18, pp. 20807–20816, Sep. 2021.

[19] X. Jin, S. Guo, J. Guo, P. Shi, M. Kawanishi, and H. Hirata, "Active suppression method of dangerous behaviors for robot-assisted vascular interventional surgery," *IEEE Trans. Instrum. Meas.*, vol. 71, 2022, Art. no. 4004809.

[20] C. Lyu et al., "A deep-learning-based guidewire compliant control method for the endovascular surgery robot," *Micromachines*, vol. 13, no. 12, p. 2237, Dec. 2022.

[21] J. Zhu, C. Wang, G. Zhang, S. A. Teng, L. Lu, and G. Teng, "A multi-stage guidewire tip tracking framework for cardiovascular robotic interventions," in *Proc. 14th Int. Congr. Image Signal Process., Biomed. Eng. Informat. (CISP-BMEI)*, 2021, pp. 1–6.

[22] K. Wang, X. Mai, H. Xu, Q. Lu, and W. Yan, "A novel SEA-based haptic force feedback master hand controller for robotic endovascular intervention system," *Int. J. Med. Robot. Comput. Assist. Surg.*, vol. 16, no. 5, pp. 1–10, 2020.

[23] Y. Zhao et al., "Surgical GAN: Towards real-time path planning for passive flexible tools in endovascular surgeries," *Neurocomputing*, vol. 500, pp. 567–580, Aug. 2022.

[24] Y. Yan, S. Guo, C. Lyu, D. Zhao, and Z. Lin, "SEA-based humanoid finger-functional parallel gripper with two actuators: PG2 gripper," *IEEE Trans. Instrum. Meas.*, vol. 72, 2023, Art. no. 3000213.

[25] Y. Yan, S. Guo, C. Yang, C. Lyu, and L. Zhang, "The PG2 gripper: An underactuated two-fingered gripper for planar manipulation," in *Proc. IEEE Int. Conf. Mechatronics Autom. (ICMA)*, Aug. 2022, pp. 680–685.

[26] I. G. Goryacheva and M. N. Dobychin, "Some results concerning the development of the molecular-mechanical theory of friction," *J. Friction Wear*, vol. 29, no. 4, pp. 243–250, Aug. 2008.

[27] P. Meijers, "The contact problem of a rigid cylinder on an elastic layer," *Appl. Sci. Res.*, vol. 18, no. 1, pp. 353–383, 1968.

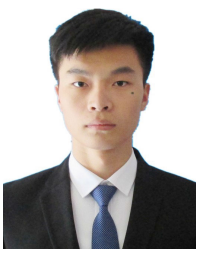

Yonggan Yan (Graduate Student Member, IEEE) received the M.S. degree in mechanical engineering from Yanshan University, Qinhuangdao, Hebei, China, in 2021. He is currently pursuing the Ph.D. degree with the Beijing Institute of Technology, Beijing, China.

His research interests include leader-follower systems for remote surgical robots.

Shuxiang Guo (Fellow, IEEE) received the Ph.D. degree in mechano-informatics and systems from Nagoya University, Nagoya, Japan, in 1995.

He is currently a Chair Professor with the Department of Electronic and Electrical Engineering, Southern University of Science and Technology, Shenzhen, Guangdong, China. He is also a Chair Professor with the Key Laboratory of Convergence System and Healthcare Technology Medical Engineering, The Ministry of Industry and Information Technology, Beijing Institute of Technology, Beijing, China. His research interests include medical robot systems, microcatheter systems, and biomimetic underwater robots.

Dr. Guo has a fellowship of The Engineering Academy of Japan.

Zhijun Lin (Graduate Student Member, IEEE) received the B.S. degree in automation from Harbin Engineering University, Harbin, China, in 2021. He is currently pursuing the master's degree in biomedical engineering with the Beijing Institute of Technology, Beijing, China.

His research interests include surgical robotics, machine learning, biomedical engineering, and automation.

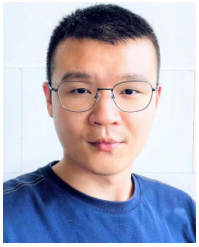

Chuqiao Lyu (Graduate Student Member, IEEE) received the M.S. degree in biomedical engineering from the Beijing Institute of Technology, Beijing, China, in 2019, where he is currently pursuing the Ph.D. degree.

His research interests include reinforcement learning, deep learning, and surgical automation.

Duohao Zhao (Graduate Student Member, IEEE) received the B.S. degree in biomedical engineering from the Beijing Institute of Technology, Beijing, China, in 2022, where he is currently pursuing the Ph.D. degree.

His research interests include robotic catheter systems for biomedical applications.

Pengfei Yang received the seven-year program of clinical medicine from the School of Medicine, Zhejiang University, Hangzhou, China, in 2007, and the M.D. degree from Second Military Medical University, Shanghai, China, 2013.

He is currently the Executive Director of the Neurovascular Center, Shanghai Changhai Hospital, Shanghai, and the Vice Director of the Institute of Cerebrovascular Diseases, the Chinese People's Liberation Army, Shanghai. His current research interests include enhanced control of hypertension and thrombectomy stroke study (ENCHANTED-2/MT), direct intra-arterial thrombectomy in order to revascularize AIS patients with large vessel occlusion efficiently in chinese tertiary hospitals: a multicenter randomized clinical trial (DIRECT-MT), managing non-acute SDH usinG ilquid materials: a chinese randomized trial of MMA treatment (MAGIC-MT), and large artery occlusion treated in extended time with mechanical thrombectomy (LATE-MT).

Yongwei Zhang received the master's degree from Second Military Medical University, Shanghai, China, in 2011.

He is currently the Vice Director of the Neurovascular Center, Shanghai Changhai Hospital, Shanghai. He is also skilled in the field of neurointerventional treatment with 20 years of experience. His representative articles have been published in the NEW ENGLAND JOURNAL OF MEDICINE (NEJM) and *The Lancet*. His current research interests include enhanced control of hypertension and thrombectomy stroke study (ENCHANTED-2/MT), direct intra-arterial thrombectomy in order to revascularize AIS patients with large vessel occlusion efficiently in chinese tertiary hospitals: a multicenter randomized clinical trial (DIRECT-MT), managing non-acute SDH usinG ilquid materials: a chinese randomized trial of MMA treatment (MAGIC-MT), and large artery occlusion treated in extended time with mechanical thrombectomy (LATE-MT).

Yongxin Zhang received the Doctor of Philosophy and Medical Doctor's degrees from Second Military Medical University, Shanghai, China, in 2017.

He is currently the Secretary of the OCIN Imaging Core-Laboratory, Shanghai. His representative articles have been published in the NEW ENGLAND JOURNAL OF MEDICINE (NEJM) and *The Lancet*. His current research interests include enhanced control of hypertension and thrombectomy stroke study (ENCHANTED-2/MT), direct intra-arterial thrombectomy in order to revascularize AIS patients with large vessel occlusion efficiently in chinese tertiary hospitals: a multicenter randomized clinical trial (DIRECT-MT), managing non-acute SDH usinG ilquid materials: a chinese randomized trial of MMA treatment (MAGIC-MT), and large artery occlusion treated in extended time with mechanical thrombectomy (LATE-MT).

Jianmin Liu received the bachelor's degree from Second Military Medical University, Shanghai, China, in 1984.

He was a Visiting Professor with the Medical College, Osaka University, Suita, Japan, in 1997. He is currently the Director of the Neurovascular Center, Shanghai Changhai Hospital, Shanghai, and the Director of the Institute of Cerebrovascular Disease of the Chinese People's Liberation Army (PLA). He has published more than 500 articles and edited and co-edited seven monographs. His current research interests include enhanced control of hypertension and thrombectomy stroke study (ENCHANTED-2/MT), direct intra-arterial thrombectomy in order to revascularize AIS patients with large vessel occlusion efficiently in chinese tertiary hospitals: a multicenter randomized clinical trial (DIRECT-MT), managing non-acute SDH usinG ilquid materials: a chinese randomized trial of MMA treatment (MAGIC-MT), and large artery occlusion treated in extended time with mechanical thrombectomy (LATE-MT).